UNIVERSITY
OF TRENTO - Italy
Department of Physics

NANOSCIENCE LABORATORY

HIGHLIGHTS 2015

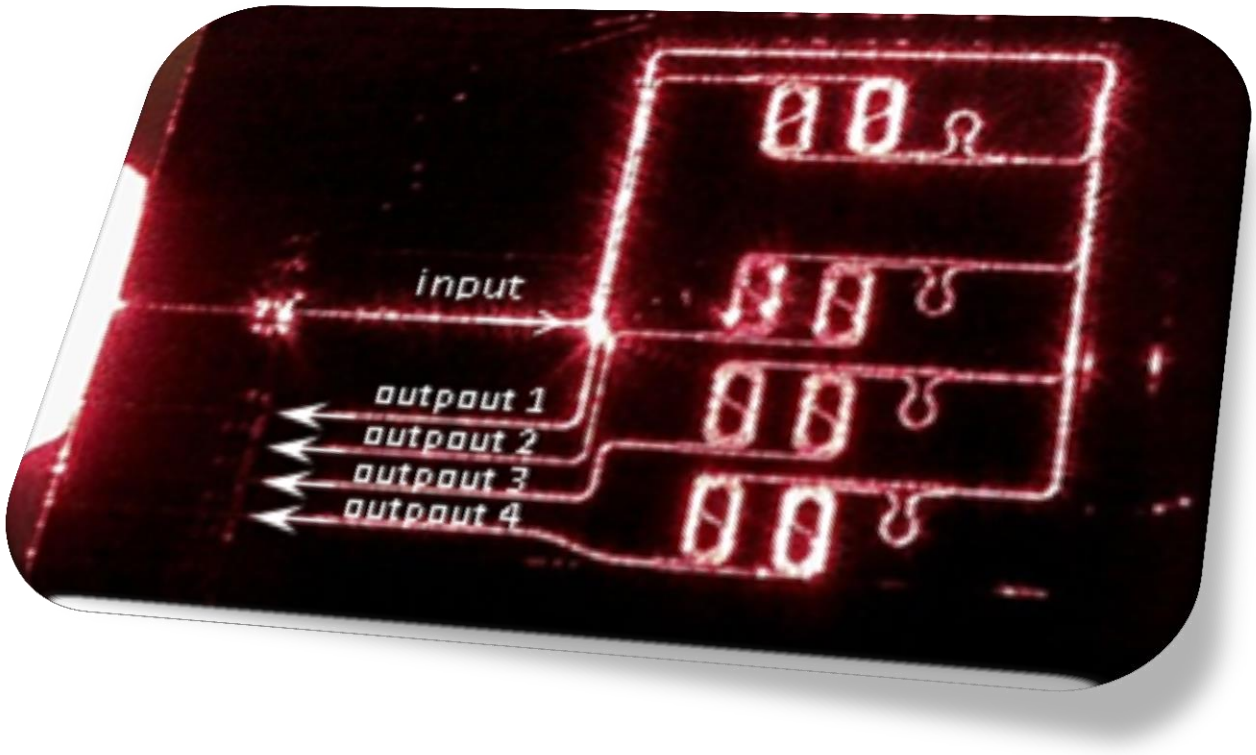

Image on the front cover:
Optical photograph of the SYMHONY photonic sensor made by four asymmetric Mach Zehnder Interferometers. In the photograph, the four interferometers are excited by visible light, which make them visible.

NANOSCIENCE LABORATORY

MEMBERS (2015)

Faculty and research staff
Lorenzo Pavesi (full professor, head)
Marina Scarpa (full professor)
Zeno Gaburro (associate professor)
Paolo Bettotti (assistant professor)
Fernando Ramiro Manzano (researcher)

Technical staff
Massimo Cazzanelli (left March 2015)
Enrico Moser
Giorgio Fontana (EP5 level)

Administrative staff
Tatsiana Yatskevich

Post-doctoral fellows
Mattia Mancinelli
Romain Guider (left October 2015)
Sanjay Thorat (left December 2015)
Santanu Mana (guest Post-Doc)

Doctoral students
Davide Gandolfi (graduated in March 2015)
Massimo Borghi
Fabio Turri
Zahra Bisadi
Stefano Tondini
Tatevik Chalyan
Alessandro Trenti
Claudio Castellan
Cecilia Ada Maestri
Chiara Piotto
Stefano Signorini

Master students
Stefano Biasi
Allegra Calabrese
Elena Chistè
Anna Lion
Sara Piccione
Francesca Marchetti

SCIENTIFIC MISSION

Introduction to the Nanoscience Laboratory

The Nanoscience Laboratory (NL) is one of the scientific groups of the Department of Physics, University of Trento. Its main area of research are nanophotonics, silicon-based photonics and nanobiotechnologies. The mission of NL is to generate new knowledge, to develop understanding and to spin-off applications from physical phenomena associated with photons and nanostructures. In particular, NL works on applying the nanoscience paradigm to silicon or silicon compatible materials to develop micro and nanosystems compatible with the main driving silicon microelectronics technologies. However, silicon is not the only material studied. Other field of interest concerns the use of polymers to tailor the properties of nanostructure atom-by-atom or the use of metals to investigate new properties which rise from plasmonics. In addition, a particular emphasis is placed on quantum photonics and its applications.

NL research group consists of more than 20 people with different scientific background. Such, researchers from physics, bio-chemistry, materials science and electrical engineering are gathered to form a group of interdisciplinary nature. It is worth mentioning that NL collaborates closely with the Center of Materials and Microsystems, Fondazione Bruno Kessler (FBK). This collaboration spans over the last twenty years and covers such topics as fabrication, testing and application of biomaterials and silicon based devices. Both parties participate in many common projects. The current ones are: project "On silicon chip quantum optics for quantum computing and secure communications – SiQuro" (financed by the Province of Trento (PAT)) and the project "Integrated SYsteM based on PHOtonic Microresonators and Microfluidic Components for rapid detectioN of toxins in milk and diarY products – SYMPHONY" (financed by the European Commission within the 7th framework). A new tight collaboration is ongoing with the Trento units of CNR-INO, specifically dedicated to implement quantum optics in a silicon integrated chip.

Moreover, with the support of FBK and CNR, every two years NL organizes a winter school on optoelectronics and photonics. The last edition was the "8th Optoelectronics and Photonics Winter School: Topolight Effects in Photonics" (March 2015). Furthermore, the members of NL are often invited to participate in the organizing committees of international conferences or workshops.

The research activities of NL are mainly supported by the local government (PAT), by the European Commission within the research frameworks, by the Italian Ministry of Education, University and Research (MIUR) and by companies. During the period covered by these Highlights, NL has been and is involved in the following projects: Project FIRB NEMATIC "Nanoporous matErials: self asseMbled blAckboard to study sTructure and InteraCtions of DNA, project SiQuro (supported by PAT within the call Grandi Progetti 2012), collaborative project Italy-India (ITPAR) supported by MIUR, some European projects within the 7th Framework: SYMPHONY (FP7-ICT-2013-10) and "Integrated Reconfigurable sIlicon phonic Switch – IRIS" (FP7-ICT-2013-11).

Silicon Nanophotonics

Silicon photonics is the technology where photonic devices are produced by standard microelectronic processes using the same paradigm of electronics: integration of a large number of devices to yield a high circuit complexity, which allows for high performances and low costs. Here, the truth is to develop photonic devices that can be easily integrated to improve the single device performance and to allow high volume production.
We are involved in researching new optical scheme for implementing optical network on a chip by using concepts of nanophotonics. We use the concept of whispering gallery modes which develops in micro-disk or micro-ring resonators to further tune the photon mode density. These disks or rings are coupled directly with narrow mode SOI (Silicon-on-Insulator) waveguides. High quality factor cavities allow studying fundamental quantum optics concept such as optical forces. Series of coupled micro-rings are studied to study chaos and resonant feedback among different rings.
To develop silicon photonics, one further add-on is making silicon do something which it is not able to do in its standard (bulk) form. Low dimensional silicon, where small silicon nanocrystals or nanoclusters (Si-nc) are developed, is one way to compel silicon to act as an active optical material. The key ingredient that makes Si-nc appealing for photonics are: quantum size effects which make new phenomena appear in silicon, such as room temperature visible photoluminescence, optical gain, coulomb blockade and multiexciton generation. Our research interests are to exploit quantum confinement and reduced dimensionality to produce quantum random number generators, nonlinear optical devices and optical amplifiers. In addition, we use strain engineering to break the crystalline symmetry of silicon and look for parametric down conversion effects.
Nonlinear optics is used to generate pairs of entangled photons which in turn feed quantum interferometers or integrated quantum photonic circuits. Here a large activity is spent in order to demonstrate in integrated devices the new properties of quantum fluid of light where the nonlinear photon-photon interaction modify the classical properties of light.

Nanobiotechnologies, antioxidants and human health

All the aspects related to the nano-bio interfaces (which are the structures where the co-existence of physical principles and biological molecules is evident) are a challenging field of research. Though the leading research concerns the design, synthesis and dynamic behavior of nanostructured bio-interfaces, more specifically we are working on three research topics: silicon- and titanium based nanosystems, single molecule detection, and antioxidant behavior in micelle systems, polymers and nanoporous structures.
To develop silicon based bio-sensors, we are currently focused on silicon based hybrid nanostructures. In particular silicon or silicon nitride flat or porous films are the starting inorganic support into which bio active layers are designed. Biological recognition elements are introduced on this hybrid layer. Molecular surface density, active layer thickness and integration of the bio-active interface with photonic devices will be the future challenges to develop the sensor system. In addition, we are developing nanostructured hybrid interfaces to capture bio-analytes and enhance their Raman signals. Gold and silver nanoparticles are used as enhancers.
Beyond traditional sensor applications, silicon nanostructures can be used as "nanosensors", which monitor the intracellular events without introducing irreversible perturbations. To this regard light emitting silicon quantum dots appear very promising. We are studying the nanoparticle coating to increase optical stability and decrease toxicity, moreover conjugation to biological molecules and strategies to increase cell uptake and control intracellular localization are future steps of this research. Titanium nanotubes showing hydroxyl-rich interfaces have been synthesized. These nanosystems are easily dispersed and stable in aqueous solutions and show a high photocatalytic activity.

Experimental facilities

The NL facilities allow for detailed experimental studies in nanoscience, photonics and biotechnologies. Since the effective collaboration with FBK most material processing and device productions are performed within their premises. For photonics, we have facilities to cover the light spectrum from the THz to UV ranges with whatever time resolution is needed. Laser sources comprehends: Ti-sapphire fs-ps laser (1 W average over 1000-700 nm, 2 ps or 70 fs pulses, 82 MHz repetition rate) interfaced with a second harmonic generator and pulse picker; Nd-Yag laser interfaced with an optical parametric oscillator which allows scanning the 400-3000 nm wavelength region (pulse 50 mJ, 10 ns, 10 Hz); TOPAS pumped with an amplified Ti:Sa laser which covers the 1-2.6 μm range with 35 fs, 10 kHz, 3 mJ; three tunable CW lasers (850-870 nm, 1200 - 1700 nm and 1500 - 1600nm) fiber pig-tailed; high power fiber-laser at 1550 nm (1-100 MHz, 50 ps); 4W EDFA and 2W semiconductors amplifiers, several pig-tailed diode lasers, ASE source at 1550 nm and a broad band SLD at 800 nm; three high-power true-CW DPSS single-line laser operating at 532, 473 and 355 nm. Detectors comprehend: visible and infrared photomultipliers and CCDs, a streak camera with ps resolution, 4K cooled bolometers which cover THz region, avalanche photodiodes for vis and IR ranges plus one capable of photon-counting in the third telecom window. IR and MIR cameras. MIR single photo counters. To perform spectral analysis several set-ups are available: FTIR and dispersive spectrophotometers, a micro-Raman setup, a micro-FTIR and a UV-vis-IR spectrophotometer (shared with other laboratories), UV-Vis and fluorescence spectrophotometer dedicated to biochemical experiments. Five dedicated apparata for WG characterization equipped with nanopositioning systems and polarization controllers are available, each one specified on a given functions: visible, infrared, pump-probe, grating coupling and non-linear measurements. Other apparata are: - visible and infrared photoconductivity set-up; - a solar simulator

for cell sizes up to 5 inches; - two nanoprobe stations (AFM and SNOM) - two semiconductor probe stations (4 and 8 inches) and many different electrical characterization set-ups (I-V, Z-Ω, EL-I, etc.). Two VIS to NIR optical spectrum analyzers are available to NL-Lab. A probe station is fiber-bunch interfaced with a spectrometer interfaced with IR and visible liquid nitrogen cooled CCDs. For sample treatment and high sensitivity analytical detection, an electrochemical laboratory equipped with several chemical hots, spinners, galvanostates and voltammeters is available. An electron beam lithography set-up (SEM attachment) is also owned. For optical, electrical and molecular dynamic simulations, the laboratory uses free and commercial software, a dedicated cluster with 16 nodes and work-stations. Two laboratories, one dedicated to chemical synthesis and the second to biological sample preparation, are also available.

2015 publications:

- P. Bettotti, C.A. Maestri, R. Guider, I. Mancini, E. Nativ-Roth, Y. Golan, M. Scarpa, "Dynamics of Hydration of Nanocellulose Films", Adv. Mater. Interf. 10.1002/admi.201500415
- R. Guider, C. Traversa, P. Bettotti, "Mechanical stress relief in porous silicon free standing membranes", Opt. Mater. Express, 5(10), 2128-2135(2015)
- P. Bettotti, N. Kumar, R. Guider, M. Scarpa, "Optical sensors based on nanoporous materials", Lecture Notes in Electrical Engineering, 319, 103-107(2015)
- F. Sgrignuoli, P. Ingenhoven, G. Pucker, V. D. Mihailetchi, E. Froner, Y. Jestin, E. Moser, G. Sánchez, and L. Pavesi "Purcell effect and luminescent downshifting in Silicon nanocrys-tals coated back-contact solar Cells", Solar Energy Materials and Solar Cells 132, 267-274 (January 2015)
- Clemens Schriever, Federica Bianco, Massimo Cazzanelli, Mher Ghulinyan, Christian Eisenschmidt, Georg Schmidt, Johannes de Boor, Alexander Schmid, Johannes Heitmann, Lorenzo Pavesi, Jòrg Schilling," Second order optical nonlinearity in silicon waveguides -inhomogeneous stress and interfaces" Advanced Optical Materials 3, 129–136 (2015)
- D. Gandolfi, F. Ramiro Manzano, F. J. Aparicio Rebollo, M. Ghulinyan, G. Pucker, L. Pavesi "Role of edge inclination in optical microdisk resonator for label-free sensing", Sensors 15, 4796-4809 (2015)
- S. Manna, R. Aluguri, R. Bar, S. Das, N. Prtljaga, L. Pavesi, and S. K. Ray, "Enhancement of photoluminescence intensity of erbium doped silica containing Ge nanocrystals: distance de-pendent interactions" Nanotechnology 26, 045202 (2015)
- Santanu Manna, F Manzano, Mher Ghulinyan, M Mancinelli, F Turri, Georg Pucker, and Lorenzo Pavesi "Multimode interference revealed by two photon absorption in silicon rich SiO2 waveguides" Applied Physics Letters 106, 071109 (2015).
- S. Tondini, G. Pucker, L. Pavesi "Spectral- and time-resolved electroluminescence of Silicon nanocrystals based Light Emitting Devices" Journal of Physics: D 48, 455103 (2015).
- L. Stefan, M. Bernard, R. Guider, G. Pucker, L. Pavesi, and M. Ghulinyan "Ultra-high Q Thin Silicon Nitride Strip-Loaded Ring Resonators" Optics Letters 40, 3316-3319 (2015).
- Romain Guider, Davide Gandolfi, Tatevik Chalyan, Laura Pasquardini, Alina Samusenko, Georg Pucker, Cecilia Pederzolli, Lorenzo Pavesi "Design and optimization of SiON ring res-nators-based biosensors for Aflatoxin M1 detection" Sensors 15, 17300-17312 (2015).
- M. Borghi, M. Mancinelli, F. Merget, J. Witzen, M. Bernard, M. Ghulinyan, G. Pucker, L. Pavesi "High frequency electro-optic measurement of strained silicon racetrack resonators" Optics Letters 40 (22) 5287-5290 (2015).
- Tatevik Chalyan, Romain Guider, Laura Pasquardini, Manuela Zanetti, Floris Falke, Erik Schreuder, Rene G. Heideman, Cecilia Pederzolli and Lorenzo Pavesi "Asymmetric Mach-Zehnder Interferometer based biosensors for Aflatoxin M1 detection", Biosensors 6(1), 1

(2016).
- M. Bernard, F. Ramiro-Manzano, N. Prtljaga, G. Pucker, L. Pavesi, I. Carusotto, M. Ghulinyan "Off-diagonal photonic Lamb shift in reactively coupled waveguide-resonator sys-tem" Proc. SPIE 9520, Integrated Photonics: Materials, Devices, and Applications III, 952006 (June 1, 2015)
- A. Samusenko, G. Pucker, D. Gandolfi, R. Guider, M. Ghulinyan. F. Ficorella, L. Pavesi "Integrated silicon photodetector for lab-on-chip sensor platforms" Proc. SPIE 9520, Integrated Photonics: Materials, Devices, and Applications III, 95200D (June 1, 2015)
- Zahra Bisadi, Alessio Meneghetti, Giorgio Fontana, Georg Pucker, Paolo Bettotti and Lorenzo Pavesi "Quantum random number generator based on silicon nanocrystals LED" Proc. SPIE 9520, Integrated Photonics: Materials, Devices, and Applications III, 952004 (2015)
- Romain Guider, Davide Gandolfi, Tatevik Chalyan, Laura Pasquardini, Alina Samusenko, Cecilia Pederzolli, Georg Pucker and Lorenzo Pavesi "Sensitivity and Limit of Detection of biosensors based on ring resonators" Sensing and BioSensing Research 6, 99–102 (2105)
- Z. Bisadi, M. Mancinelli, S. Manna, S. Tondini, M. Bernard, A. Samusenko, M. Ghulinyan, G. Fontana, P. Bettotti, F. Ramiro-Manzano, G. Pucker, L. Pavesi "Silicon nanocrystals as enabler for nonlinear optics and secure communications" feature article submitted to Physica Status Solidi A 212, No. 12, 2659–2671 (2015).
- Jörg Schilling, Clemens Schriever, Federica Bianco, Massimo Cazzanelli and Lorenzo Pavesi "Second order nonlinearity in Si by inhomogeneous strain and electric fields", Proc. SPIE 9546, Active Photonic Materials VII, 95461T (August 31, 2015).
- M. Borghi, D. Gandolfi, M. Ghulinyan, R. Guider, M. Mancinelli, G. Pucker, F. Ramiro-Manzano, F. Turri, and L. Pavesi, "Silicon Microresonators: How to Give a New Twist to Sili-con Photonics," Chapter 2 in New Horizons in Nanoscience and Engineering, D. L. Andrews and J. G. Grote, Eds., SPIE Press, Bellingham, Washington, pp. 37-85 (2015).
- Z. Gaburro, N. Daldosso, and L. Pavesi, Porous Silicon. In: Saleem Hashmi (editor-in-chief), Reference Module in Materials Science and Materials Engineering. Oxford: Elsevier; 2016. pp. 1-11

2015 book:

- Light Localisation and Lasing: Random and Pseudorandom Photonic Structures Mher Ghulinyan and Lorenzo Pavesi editors, Cambridge University Press (2015)
- Silicon Photonics III: Systems and Applications, Lorenzo Pavesi and David J. Lockwood editors, Topics in Applied Physics vol 122 (2016)

2015 PhD Thesis:

Davide Gandolfi "On-chip photonic label-free biosensors" (30th of March, 2015)

1. Towards quantum optics experiments in the mid-infrared
(Alessandro Trenti)

The mid-infrared is emerging as an interesting field in photonics for several applications, such as gas analysis and medical diagnostics. Modern quantum cascade lasers have evolved as ideal coherent mid-infrared excitation sources, but simple, low-noise, room-temperature detectors and imaging systems lag behind. The Technical University of Denmark (DTU) has recently developed a novel upconversion system for sensitive, two-dimensional mid-infrared single photon spectral imaging [1]. The NanoLab has started a collaboration with DTU within the SiQuro project and two mid-IR up-conversion modules, for use in combination with silicon based single photon counters, are currently available in the Nanoscience Laboratory. Thanks to this new tool, it is possible to extend experiments of quantum optics from the third telecom window to the mid-infrared part of the spectrum, up to about 5 μm.
An experimental set-up was built: the source is a ps pulsed laser @ 1.55 μm (7W of maximum average power) which is focused on a 1-cm long Periodically Poled Lithium Niobate Crystal (PPLN). This nonlinear crystal generates, through Spontaneous Parametric Down Conversion, type-0 pairs of entangled photons near the degenerate wavelength of 3.1 μm. Due to the intrinsic low efficiency of the process (around -100 dB) one needs a mid-infrared single photon counter in order to detect the generated photon pairs. This is achieved thanks to the up-converter module coupled to visible single photon detectors.

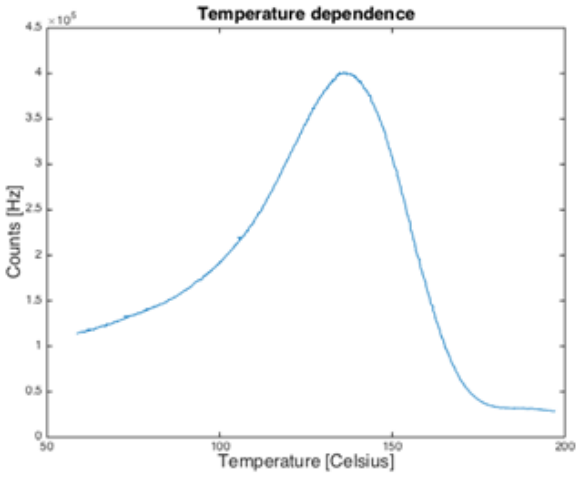

Figure 1. *Spectrum of the generated MIR photons through SPDC as a function of the temperature of the up-converter module, i.e. the phase matched wavelength.*

Preliminary measurements are shown in fig 1. Here, the count rate of the silicon based Single Photon Counting Module is reported as a function of the temperature of the up-converter module. Since there is a one to one correspondence between temperature and phase-matched wavelength, this is actually the spectrum of the generated radiation from the PPLN, which shows the typical bell shape around the degenerate wavelength of 3.1 μm.
In the near future, we will proceeded to assess the correlated properties of the photon pairs. One approach is to perform a typical coincidence measurement [2], with the help of two up-converter model coupled to two single photon counter. Up to our knowledge, nobody was able to show a coincidence measurement in the mid-infrared so far.

References
1. Jeppe Seidelin Dam, Peter Tidemand-Lichtenberg and Christian Pedersen, "Room temperature mid-infrared single-photon spectral imaging", *Nature Photonics*, **6**, (2012).
2. Alessandro Trenti, Massimo Borghi, Mattia Mancinelli, Giorgio Fontana and Lorenzo Pavesi, "One and Two Photon Quantum Interference in a Mach-Zehnder Interferometer", unpublished.

2. A system for photon counting in the MIR
(Mattia Mancinelli, Sara Piccione)

The up-conversion module is based on sum frequency generation (SFG) that takes place within a laser cavity. The system is capable to up-convert both coherent and incoherent mid infrared light (MIR) at around 3um to 0.780 um with a quantum efficiency (QE) of up to 80%. This high QE is given by the intra-cavity high circulating power (100 W CW) and the low loss cavity design that allows reaching high quality factors.

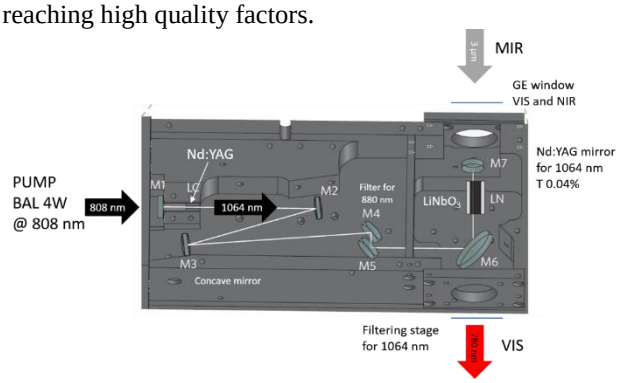

Figure 2. *Laser cavity scheme of the up-conversion module.*

Figure 2 reports the laser cavity scheme of the module. A broad area laser diode (BAL) at 880 nm act as the pump for the Nd:Yag crystal. The cavity is composed of a folded Fabry-Perot cavity that starts at M1 and ends at M7. All the mirrors are hard coated to reflect just the 1064 nm line emitted by the crystal. The coating of M7 is deposited on a Nd:Yag substrate to ensure transparency to MIR light. M4 and M5 compose a filter stage for the 880 nm and are placed in a separated black chamber. The non-linear crystal (LN) is placed in front of the input window of the MIR light. The proper beam waist within the LN is selected by the concave mirror M3. A germanium filter is placed on the input mirror to keep the system free of visible light. The MIR light travels into the crystal and is up converted at 780 nm. Then, the up-converted light can pass the mirror M6 and exits from the output window (VIS). The output mirror is equipped with a set of dichroic filters to cut out the high 1064 nm laser line. The up-converted MIR signal can be detected both with a visible camera or a visible photon counter.
In order to fully understand the modules behavior, preliminary tests has been performed. The module up-conversion

efficiency is linked to the intra-cavity power (pump) that will be mixed with the input MIR light. Therefore a measure of the pump power as a function of time and as a function of the pump diode current as been performed.

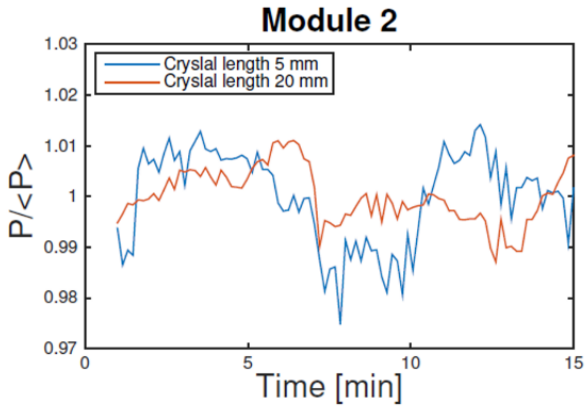

Figure 3: *Fluctuations of the intra-cavity power normalized with respect to the mean value, for both the modules, and using the two crystals. The mean power is 62W. The injection current of the pump diode was 3.2A.*

As can be seen from fig. 3, the pump power has time fluctuations that come from the presence of a power dependent loss generated by the non-linear crystal.

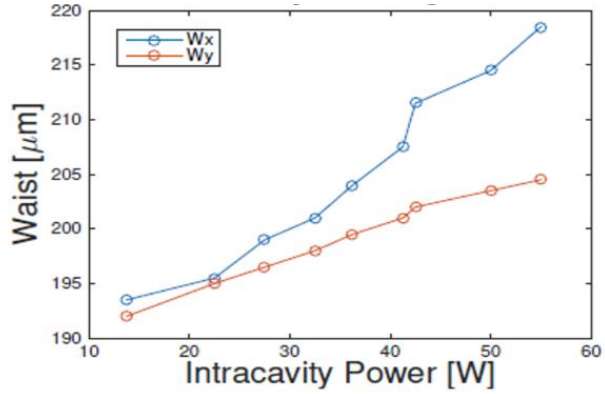

Figure 4: *Beam Waist along the x and y directions as a function of the cavity power.*

Figure 4 reports the pump beam waist (Gaussian waist) as a function of the cavity power. There is a small increase of the waist due to the thermal lens effect. These measurements tell us that it is possible to reach an intensity of 40 kW/cm^2. By measuring the ratio between the input MIR power (black body source) to the up-converted visible light it is possible to extract the conversion efficiency.
Thanks to the very intense cavity power and a very long crystal it is possible to achieve a conversion efficiency as high as 40%, as reported in fig. 5. The poling period inside the non-linear crystal inside the cavity allows to phase match only a specific band from the MIR to the visible. With this respect the poling acts as a grating and allows performing also the spectrum of the up-converted radiation. The spectrum is measured by changing the crystal temperature and thus its refractive index (phase matching condition).

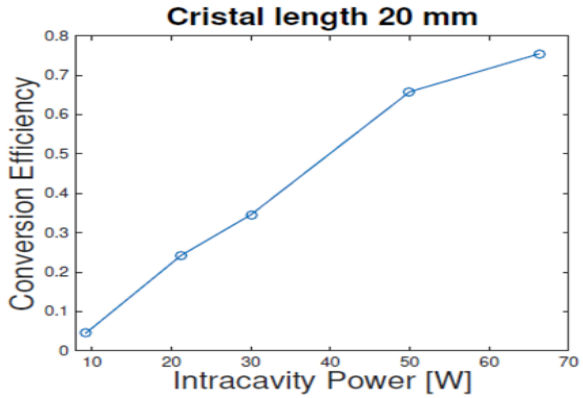

Figure 5*: Conversion efficiency as a function of the intra-cavity power.*

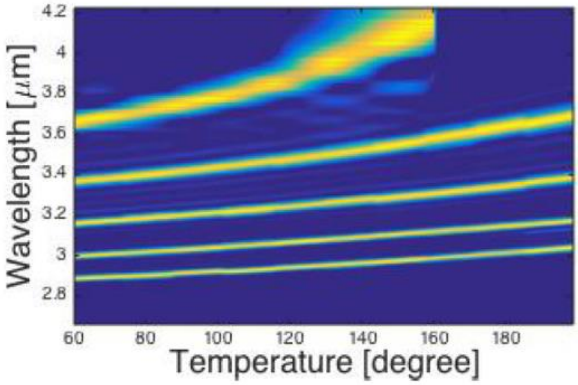

Figure 6*: Power converted via difference frequency generation and down-converted wavelength as a function the LiN crystal temperature. The curves were collected for all the different poling periods in the LiN crystal which are to 21 um, 21.5 um, 22 um, 22.5 um, 23 um (from the bottom to the top).*

Figure 6 reports the measured spectral response of the module for five poling periods. The measurement has been done by means of a tunable visible laser and an InSb MIR detector to monitor the down-converted radiation. The phase matched visible wavelength can be calculated by the conservation of energy. As can be seen by changing the poling period and the temperature it is possible to cover the 2.9 um to 4.2 um MIR region. With this tool, it is possible to perform spectra at the level of single photons (fW) at room temperature; therefore it will be possible to measure also the spectrum of the spontaneous down converted radiation.

3. Microrings and Mach Zehnder based biosensors for Aflatoxin M1 detection in milk (Tatevik Chalyan)

Since November 2013, we are involved in the European Project SYMPHONY. The project aims to produce a platform that enables the rapid detection of toxins and contaminants, with an initial focus on the carcinogen Aflatoxin M1, in milk and milk products.
High-resolution biosensors, such as SiN asymmetric Mach-Zehnder interferometers (aMZI developed by LioniX) and SiON microring resonators (MRR developed by

UniTN and FBK), were studied by our group for analyte detection. Both types of sensors gave good results in terms of sensitivity, Limit of Detection and reproducibility. The aMZI solution was selected for final implementation because it was demonstrated to be more suitable for the integration steps. Figure 7 shows the final design of aMZI chip.

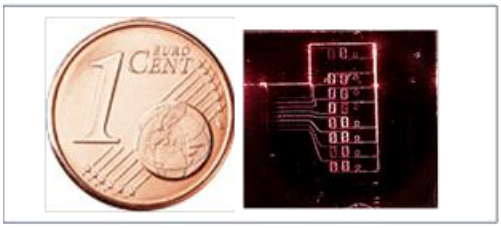

Figure 7. *Picture of the aMZI chip. See also the cover page*

For these sensors were measured a Limit Of Detection (LOD) of $4.5x10^{-7}$ Refractive Index Units (RIU) and a sensitivity of 15600 rad/RIU. Different strategies for surface functionalization, based on aptamers and antibodies fragments (Fab') were tested.
The aptamer layer captured around 10^{13} aflatoxin molecules per cm^2, matching the requirements to achieve the lowest limit of detection in EU regulation

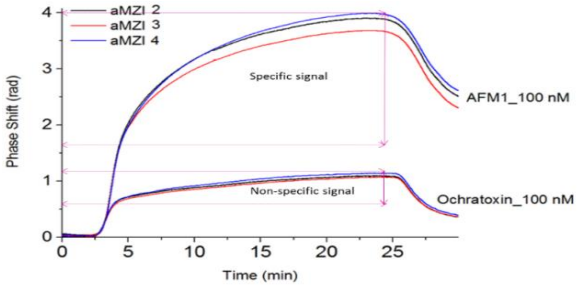

Figure 8. *Sensorgram recorded on three aMZI sensors by flowing AFM1 (top) and Ochratoxin (bottom) through the microfluidic chamber.*

Figure 8 shows the measurements for three sensors when a 100 nM concentration of Aflatoxin M1 or of Ochratoxin is added to the buffer solution. The phases shift in time following the kinetic of the binding of the toxins to the antibody on the surface of the exposed aMZI arms. The functionalization is specific. In fact, in the case of AFM1, after MES rinsing, the phase shift is 2 radians larger than the one before the toxin injection, while in the case of Ochratoxin it is only about 0.25 radians after rinsing the sample.

4. Robust random number generation via an all-silicon-based approach (Zahra Bisadi, Giorgio Fontana)

Modern cryptographic techniques require sequences of high quality random numbers to encrypt and decrypt secret information. A lot of research has been done for the generation of random numbers through physical, non algorithmic methods. Quantum mechanics, with the uncertainty and unpredictability in quantum phenomena has helped to develop efficient methods to produce unique, high quality random numbers. However, most approaches need to apply post-processing operations to the raw data in order to keep the quality of random numbers high enough for the cryptographic purposes. Here, we focused on a random number generation technique in which the source of entropy is quantum mechanical. We prepared a simple experimental setup based on photon arrival time measurements with thorough consideration of the detector imperfections. The entropy source is a Si nanocrystals (Si-NCs) light emitting diode (LED) coupled with a silicon single photon avalanche diode (SPAD) detector. A dedicated field-programmable data array (FPGA) performs the random bit extraction. This approach avoids the use of post-processing algorithms. The proposed QRNG is robust against variations of the internal and external parameters such as the aging of the components and changing temperature.
The Si-NCs LED has a metal oxide semiconductor (MOS) structure with a graded-size multilayer as the active layer. Emission occurs in the visible range and can be detected by Si photodetectors. Photons emitted from the Si-NCs LED follow a nearly ideal Poisson distribution. The Poisson process has the property that if there is only one single arrival in a time interval, the distribution of the arrival times is uniform in the interval. Therefore, we consider intervals with a fixed duration having only one single arrival; intervals with no arrival or with more than one arrival are discarded. Based on this, our main goals of robustness and full modeling of the QRNG will be achieved. The experimental setup is presented in fig. 9. Photons emitted from a Si-NCs LED are detected by a single photon counting module through a multimode fiber bundle. The measurement of the arrival times is performed by a fully synchronous logic in an FPGA.
Sequences of data were obtained and analyzed for randomness. The raw data (acquired at different applied currents to the LED and different temperatures) show high quality of randomness and passed all the statistical NIST tests without the application of any post-processing algorithms. The maximum bit-rate is 1.68 Mbps with the efficiency of 4-bits per detected photon.

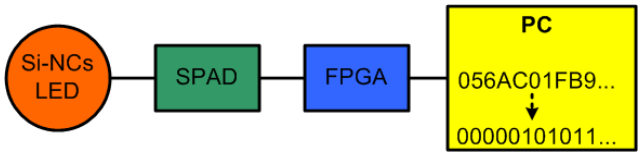

Figure 9. *Schematic of the setup for random number generation.*

5. Modelling and validation of high-performance and athermal AWGs for the silicon photonics platform (Stefano Tondini, Claudio Castellan and Mattia Mancinelli)

In the Wavelength Division Multiplexing (WDM) scheme, multiple sources are modulated and encoded to carry optical signals. Array waveguide gratings (AWGs) are a key component in WDM systems, allowing for demultiplexing and routing of wavelength channels. In order to improve the design of a silicon on insulator (SOI) AWG

able to get over the performances achieved so far, we modified the star coupler (SC) stage and searched a-thermal geometries and dedicated heating systems (fig.10 (a)).
We evaluated how the background noise is modified within a whiskered-shaped star coupler (SC) optimized to reduce the reflectivity of the SOI slab/silica interface and keep down back-scattered optical signal. The novelty of our approach consists in placing, perpendicularly to the focal lines, a series of tapered waveguides that end in a particular geometry acting as "reflection killers" (fig. 10 (b)). The study has been carried out by analyzing the Fabry-Perot interference that arises between the input focal line of the SC and the output facet of a waveguide [1]. By evaluating the Fourier Transform of the optical signal, we compared the whiskered SC with the usual one. The experimental results are in a good agreement with the numerical simulations. We achieved suppression of the edge-reflected light in the whiskered SC improved by more than one order of magnitude with respect to a standard SC (fig.10 (c)).

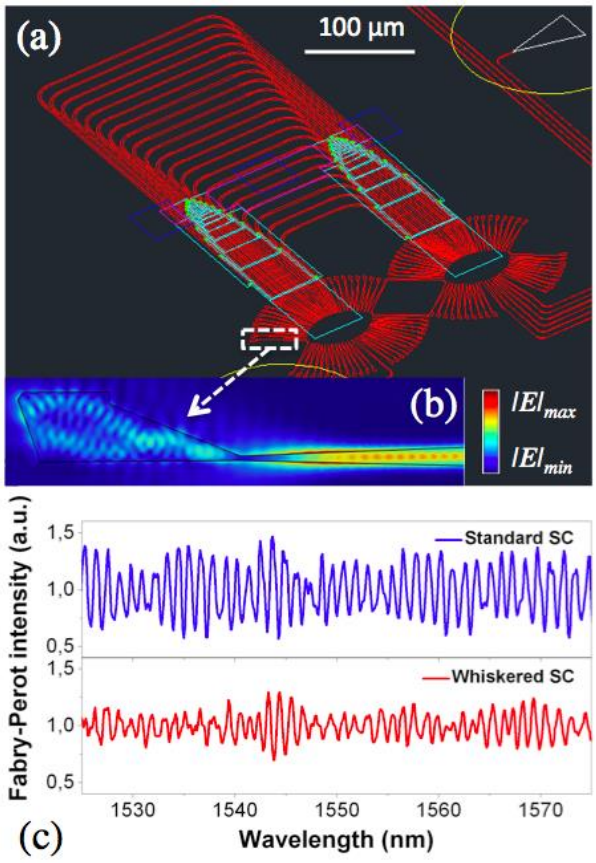

Figure 10. *(a) Whiskered star coupler AWG layout. Each color represents a different design layer: in red the silicon waveguides, in cyan Ti/TiN heaters, in green the copper pillars, in blue the electrical pads. (b) FEM simulation of the electric field profile propagating through a reflection killer of one whiskered SC. Back-reflections are about -18 dB. (c) Fabry-Perot interference evaluated by a tunable IR laser within both a standard SC AWG (blue solid line) and a whiskered SC AWG (red solid line).*

We committed in adjusting the temperature-dependent wavelength shift that the waveguides undergo when a temperature variation is experienced by the AWG. We simulated and realized a design using a cladding material with a negative thermo-optic coefficient. By means of a TiO2 covering [2], we reduced the thermal sensitivity of the whole device. This approach allows for coping with possible thermal-induced environmental changes, especially in the case of the integration of the AWG within an EPIC.
We dimensioned a heating circuit that allows the fine-tuning of the AWG channel-output. By applying specific phase-shifts on each single waveguide of the array, we have been able to move the FSR without affecting the channel spacing. The suggested geometry minimizes the power consumption needed to obtain a wavelength-shift in the output spectrum and results in the first attempt to a high-performance and CMOS compatible heater for AWGs.

References

1. S. Chen, Q. Yan, Q. Xu, Z. Fan, and J. Liu, "Optical waveguide propagation loss measurement using multiple reflections method," Optics communications, 2005, 256, pp. 68-72.
2. J.M. Lee, "Influence of titania cladding on SOI grating coupler and 5µm-radius ring resonator," Optics Communications, 2015, 338, pp. 101-105.

6. Are Porous Silicon Substrates Suitable for Mass Spectrometry?

(Chiara Piotto, Paolo Bettotti)

Mass spectrometry (MS) is a technique exploited for the analysis of chemical compounds and in recent times, various nanostructured substrates have been introduced to improve this method; among them, we focused our attention on porous silicon (PSi) chips [1]. Since PSi substrates have been introduced [2], several researchers explored the PSi characteristics (pore diameter, layer depth, porosity, extent of oxidation) that optimize their use for MS analysis but they came to conflicting results.

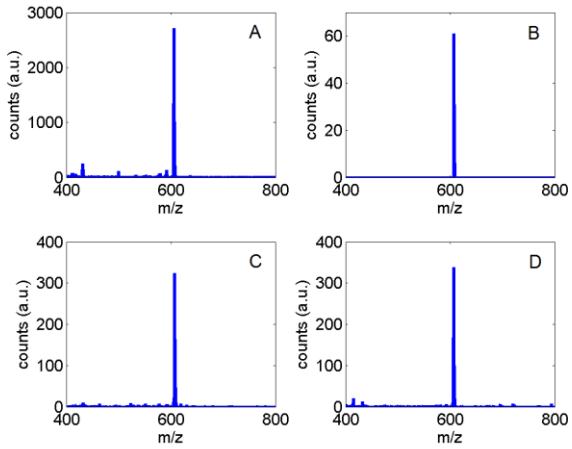

Figure 11. *Spectra acquired analyzing Reserpine (monoisotopic peak at 609.6 D a) on different substrates. A: PSi+HF; B: PFPPDCS-bulk-Si; C: PFPPDCS-porous alumina; D: PFPPDCS-bulk-aluminum.*

In order to shine light on some these vagues aspects, we prepared hundreds of PSi samples differing in their morphology and surface properties. After the etching proce-

dure and before depositing the analyte all the samples were thoroughly rinsed in EtOH. No signal were obtained from any of these samples. On the contrary, we found that MALDI signal was reproducibly obtained only from those chips that were poorly washed after the etching and that, probably, contain residual HF inside the pores (see fig. 11A). We noticed that only HF traces ease the molecular ionization, while other acids (such as CH3COOH or HCl) do not play any role on the desorption. These results suggest that the nanostructured surfaces themselves are not sufficient for the analytes protonation and that the F- presence is crucial.

Several literature results reported that the performance of the PSi substrates can be improved tailoring their surface properties. In particular several works report the used of (3-Pentafluorophenyl)propyldimethylchlorosilane (PFPPDCS) to increase the S/N ratio. We notice the same effect on our PSi samples but, unexpectedly, we get similar detection limits also on PFPPDCS functionalized bulk-Si substrates (see fig. 11B).

Thus, we conclude that when naked-PSi chips are used, the fundamental role of the nanostructures is to hold HF traces inside the pores. However, when dealing with PFPPDCS-samples, the nanostructuring is not necessary for the desorption/ionization processes: it is the PFPPDCS to play a crucial role. We exclude a role of the silane in the UV light absorption because its molar absorption coefficient at 337 nm is around 5 L/(cm/mol), orders of magnitude lower than that of typical MALDI matrices).

Moreover we found that other materials are suitable substrates for MS once they are functionalized with PFPPDCS. In fact, we were able to detect analytes using also porous alumina (see fig. 11C) and bulk aluminum (see fig. 11D).

The fact that no signal came from the PFPPDCS-ITO suggest a role of the substrate underlying the silane layer: proper chips for MALDI have to be both electrical conductors and UV absorbers.

Summarizing, the experiments showed that analytes can be detected using naked-PSi chips only if some residual HF is present within the pores. If PFPPDCS is used to functionalize the chip surfaces then nanostructuring has no role in the analytes detection. Our results also suggest that the materials, which are both electrical conductors and UV light absorbers, can be silanized with PFPPDCS to be exploited as suitable substrates for MS.

References

1. C. Piotto. "*Are Porous Silicon Substrates Suitable for Mass Spectrometry*?" University of Trento, Final Thesis, 2014-2015

2. J. Wei, J. M. Buriak, and G. Siuzdak. "*Desorption–ionization mass spectrometry on porous silicon*." Nature, 399: 243-246, 1999.

7. Mechanical actuator based on nanocellulose fibers (Paolo Bettotti, Cecilia Ada Maestri, Romain Guider and Marina Scarpa)

The design of materials capable of mechanical responses to physical and chemical stimuli represents one of the most exciting and challenging areas of scientific research because of the huge number of their potential applications.

Among the very broad types of materials and approaches currently investigated, much interesting for bio-applications are those that use water to induce changes of the conformations of the molecular components. Nature, and cellulose-based organisms in particular, provide many examples of actuation mechanisms based on hygroscopic processes that can be used to design artificial analogous with a predetermined mechanical behavior.

We investigated the molecular events occurring in thin films of carboxylated nanocellulose fibers, which are able of converting water gradients into mechanical bending movements at the macroscopic scale thanks to an interface-driven water sorption process (fig. 12).

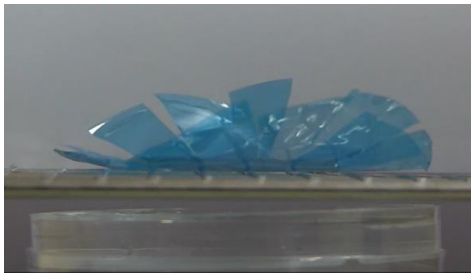

Figure 12. *Actuation movement of carboxylated nanocellulose films exposed to a water gradient. The films show an apparent hydrophobic repulsion and bend keeping the exposed side far from water.*

The analysis of the mechano-actuation showed that the film movement is fast and reproducible. The actuation responds to water gradients, but not to changes in the environmental humidity; it does not respond to gradients of non-polar solvents and is scarcely activated by polar organic solvents. Unlike many actuation mechanisms, for which a relationship between stimulus amplitude and response intensity holds, nanocellulose films transduce gradient intensity into rate of displacement. This relationship is quantitative and the response was observed at vapor pressures as low as 1.2 mmHg .

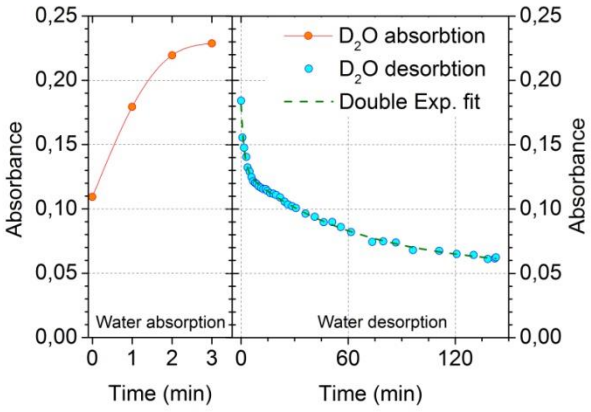

Figure 13. *Dynamics of both absorption (left) and desorption (right) of D2O from NC film.*

The observed actuation was associated to an efficient and reversible water sorption process by the hydrophilic nanocellulose fibers at the film interface. Spectroscopic data

indicate that water desorption is, conversely, slow and follows a kinetic behavior supporting the presence of two binding sites for water molecules within the fibril network (fig. 13).
The mechanical origin of the bending was difficult to be measured directly because of its dynamic nature and the need of keeping a humidity gradient across the film. AFM images and spectroscopic data suggested that the adsorbed water induces swelling of the superficial nanocellulose layers and local structural re-arrangement, however transitions between ordered and random coil conformations were not observed.
The understanding of this actuation mechanism offers exciting opportunities to design fast and efficient actuators based on a common, renewable and biocompatible material.

References

1. Dynamics of Hydration of Nanocellulose Films P.Bettotti, C. A. Maestri, R. Guider, I. Mancini, E. Nativ-Roth, Y. Golan, M. Scarpa, Adv. Mater. Interf., 10.1002/admi.201500415

8. Modeling the propagation of ultra-short pulses in silicon waveguides: second and third order nonlinear effects

(Claudio Castellan, Mattia Mancinelli)

It is well known that centrosymmetric materials does not show any second order nonlinear effect, since for these materials all the components of the second order nonlinear susceptibility tensor are zero. Therefore, second order nonlinear effects cannot be measured in silicon waveguides, since it is a centrosymmetric material. However, some of the components of this tensor are expected to be activated by externally induced stresses, that can be achieved by the deposition over the waveguide of a stressing material (such as silicon nitride) or by mechanically deformation. The problem of detecting second order effects in strained silicon waveguides comes from the fact that silicon is characterized by an intense third order nonlinearity. Therefore, looking for second order nonlinear phenomena one is often annoyed by the presence of third order effects.
Both the second and the third order effects are strictly correlated to many experimental parameters, such as the laser power, the pulse temporal duration, and the wavelength value. Therefore, we developed a numerical simulation able to describe the propagation of optical pulses in silicon waveguides, in order to determine the experimental parameters that allow for minimizing the third order effects. Our model considers both the second order effects (in our case, the Second Harmonic Generation) and the third order effects (such as Self Phase Modulation, Two Photon Absorption, and so on). Since we often deal with ultra-short pulses (whose temporal width is around 100 fs – 1 ps), our model accounts also for the temporal evolution of the pulse in the waveguide.
Some of the second- and third-order nonlinear effects coming from our simulation are shown in fig. 14. In figure 14(a) it is shown the spectral broadening a pulse under the effect of the Self Phase Modulation. Being the spectral bandwidth of the second order phenomena very narrow, this fact should be avoided. A possibility for doing that is reducing the temporal width of the pulse. In fig. 14(b) it is shown the time evolution of a pulse propagating in the waveguide, that gives rise to the generation by Second Harmonic Generation of the pulse shown in fig. 14(c). The generated pulse shows a temporal broadening in the propagation through the waveguide, due to the difference in the group velocity between the generated pulse and the pump signal. This phenomenon is known as walk-off, and becomes more apparent for shorter pulses.
The experimental validation of this model will take place in the next months. With the most performing experimental parameters and assuming a second-order nonlinear susceptibility of 0.01 pm/V, the efficiency of the generated pulse is expected to be around -120 dBm.

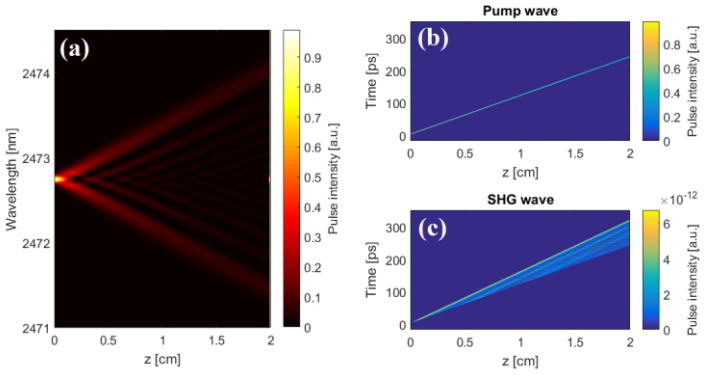

Figure 14. *(a) Spectral broadening of a Gaussian-shaped pulse under the effect of the Self Phase Modulation. The pulse propagates in a waveguide along the propagation direction z, and its temporal width is around 80 ps. (b) Time evolution of a Gaussian pulse (temporal width 1 ps) centered at 2472 nm. (c) Time evolution of the Second Harmonic wave generated by the pulse in (b) at 1236 nm. We assume a second-order nonlinear susceptibility of 0.01 pm/V.*

9. Three new elements for a fast, easy and clean experiment: application to a Fully-Automatized free-space pump and probe phase measurements

(Stefano Biasi, Fabio Turri, Fernando Ramiro-Manzano)

The realization of an experiment in photonics can be roughly divided in three main steps:

1. Design of the photonics device/chip;
2. Set-up implementation and measurements;
3. Analysis of the results;

Here we propose three different tools, which are able to simplify the realization of these steps.
For the design of the chip, we created a graphical interface able to provide the user with a final .gds file containing all the requested structures. Several devices (all pass / add drop rings, bent/straight waveguides, directional couplers, etc.) are already present in the program library: they can be inserted directly from the user interface (fig. 15) or from a script file by specifying their parameters (dimensions, input/output ports, layer, etc.). Moreover, the user with a simple Matlab script can edit new custom structures and insert them in the chip design. The first application of this

tool was the design of an entire mask for the observation of phase variation in several photonic structures (ring resonators, straight and bent waveguides, etc.). Indeed, the manifestation of several phenomena can be revealed by looking at the phase shift undergone by light when travelling along some specific optical path [1].

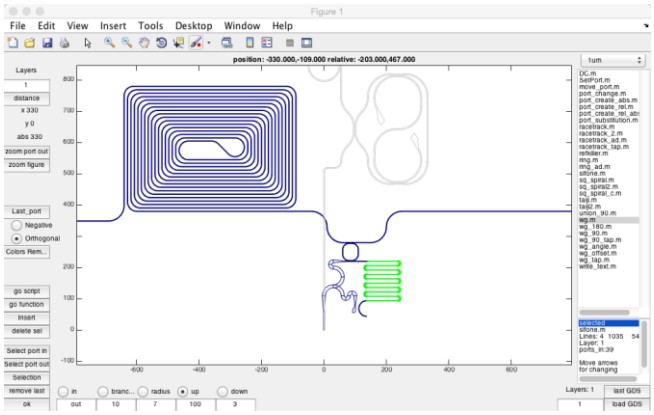

Figure 15. *Graphical interface of the design program with two layers (blue and grey) presenting waveguides and rings with complicated and customized shapes (in green the last selected input)*

To measure the phase, we built a fully automatized set-up, based on a free-space Mach-Zehnder interferometer, able to work both on integrated or bulk optics samples.

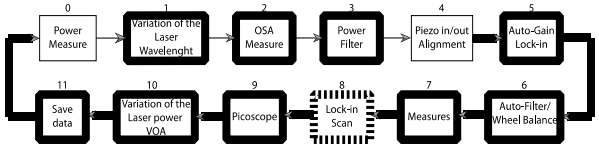

Figure 16. *Flowchart of the automatized system: each one of the twelve stages can be enabled or not providing fast and easy creation of a personal measurement procedure*

The basic interferometer, with the device to be tested placed in one of its arm, follows a computer controlled scheduler routine (see fig. 16), which allows the user to end up with transmittance and phase measurements. The only manual task is the rough first alignment and the selection of the acquisition mode. Indeed, several possibilities are given (in input: scan along different input powers and/or wavelengths, align the stage at each run, perform repeated data acquisition to obtain mean values; in output: measure input power through a thermopile and/or acquire the spectrum from an OSA) which makes the set-up easily configurable for specific tasks. The main characteristic of the set-up is the employment of a modulated laser signal (using a chopper) at the input and of a lock-in amplifier at the detection stage. This brings two advantages: first, the signal to noise ratio is largely increased because the lock-in filters out the white noise, this results in very clean spectrum, even with very low signal powers; second, the system is designed to perform phase measurements in a pump and probe configuration where the pump is continuous wave which allows to filter it out with the lock-in.

10. Mode selection and four wave mixing in a multimode silicon waveguide

(Stefano Signorini, Massimo Borghi, Mattia Mancinelli)

Four Wave Mixing (FWM) is one of the most implemented nonlinear optical processes for on chip entangled photons generation, wavelength conversion, Optical Parametric Amplification and Optical Parametric Oscillation. The generation or the amplification of two frequencies, called the idler and the signal, which collinearly propagate with an intense pump beam along the same waveguide, characterize this process. The efficiency of the FWM process depends on momentum conservation, which depends on the chromatic dispersion of the modal effective index. In silicon waveguides, it is possible to engineer the chromatic dispersion by changing their cross section, thus making the momentum conservation possible. As the effective index depends also on the waveguide mode order, it is possible to make the different FWM frequencies propagating in different waveguide modes, to achieve the momentum conservation. To accomplish this task a system able to selectively excite modes in the waveguide is needed. The idea is to couple light into the waveguide through an interference pattern, which can be tuned at will, in order to select the excited mode inside the guiding structure. In fact, if the interference pattern at the input of the waveguide is made equal to the profile of a certain guided mode, light will propagate in waveguide mainly on that particular mode.

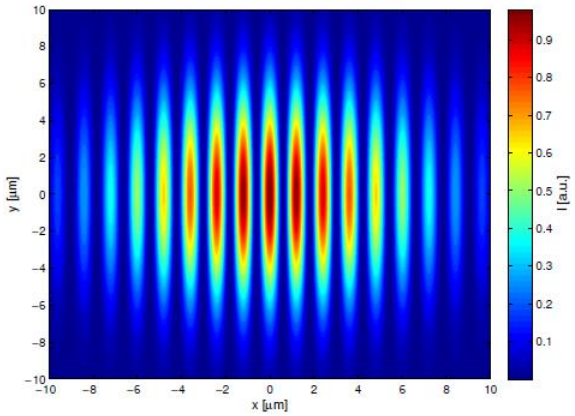

Figure 17. *Simulation for the 2D interference pattern arising from the intersection of two coherent beams.*

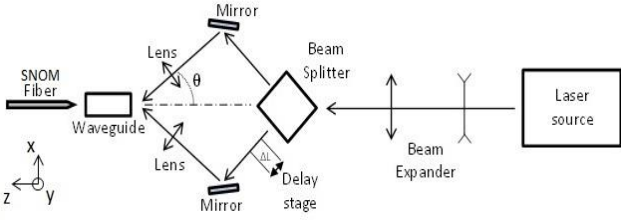

Figure 18. *Interferometer set up for mode selection in waveguide*

In the system implemented, the interference, shown in fig. 17, arises from the intersection of two coherent beams that travels tilted by an angle, as shown in fig. 18 where the

experimental set up adopted is reported. By tuning the angle θ it is possible to control the period of the interference pattern. The selection of modes in waveguide with the interferometer set up was successfully verified. However, due to the high coupling losses, another set up was developed. This was characterized by a single fibre, which was tilted by an angle with respect to the waveguide input facet. By changing the angle, the field profile is tuned and a selection of the excited mode in the waveguide is made possible. This second approach was less effective in mode selectivity, but allowed for a higher coupled power.

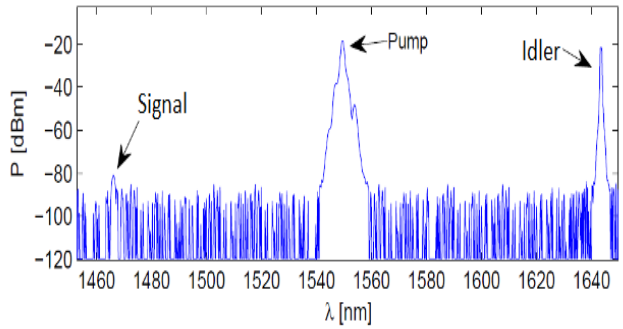

Figure 19. *Example of a spectrum for Stimulated FWM*

With this second set up Stimulated FWM was successfully achieved, and, in fig. 19, a spectrum is reported. Here, a wavelength conversion of 178 nm is obtained from the idler at 1644 nm to the signal at 1466 nm, with an efficiency of -37 dB. The efficiency has to be evaluated considering the peak power of the generated signal, since the pump beam is a pulsed laser at 10 MHz with a pulse width of 40 ps. The best result for Stimulated FWM with the described experimental approach was a wavelength conversion of 187 nm with -20 dB in efficiency.

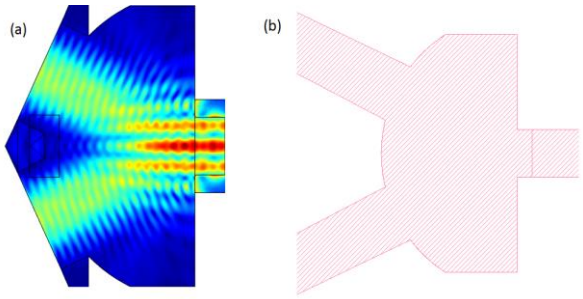

Figure 20. *(a) FEM simulation for the integrated interferometer exhibiting a third order mode selection in waveguide. (b) Example of the design of the integrated interferometer.*

These measurements were obtained with a macroscopic apparatus, and the next step is to further improve the efficiency of FWM by integrating the interferometer system on chip, following the design in fig. 20, for the generation of entangled photon pairs via Spontaneous FWM. The interferometer approach to mode selection should guarantee a greater robustness to fabrication defects with respect to phase matching based devices, especially for those applications that involve a broadband wavelength conversion.

11. Time resolved electro-optic measurement of strained Silicon waveguides (Massimo Borghi)

The linear electro-optic effect (or Pockels effect), that is the change of the refractive index because of an applied electric field, is absent Silicon. This is due to Si symmetry. The enabling of a second-order nonlinear optical susceptibility χ^2 in Si could be instrumental to the realization of ultrafast integrated electro-optic modulators. More generally, the presence of an appreciable χ^2 in Si would validate the Silicon-On-Insulator (SOI) platform as an alternative to Lithium Niobate for second-order nonlinear optics. In the last few years, strained Silicon has been proposed as a potential electro-optic material [1]. The centrosymmetry of the crystal is broken by a stressing film, usually Silicon Nitride (SiN), which is deposited on the top of the waveguides. By using this approach, several demonstrations of electro-optic modulation have been reported [2,3]. Typically, the value of the strain induced χ^2 ranged from $15\ pmV^{-1}$ [1] to $336\ pmV^{-1}$ [3]. As recently reported, these values could have been overestimated due to the contribution of free carriers to the electro-optic modulation, which are released by the trap states located at the interface between Si and SiN [4].

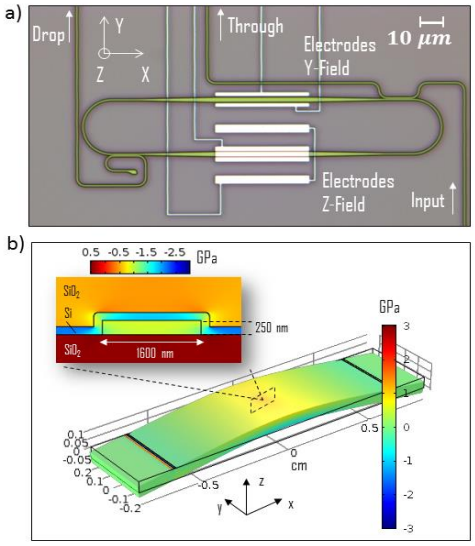

Figure 21. *(a) Optical microscope image of the racetrack resonator. A voltage is applied between the set of electrodes (in white) indicated as Electrodes Z-Field. (b) Finite Element Method simulation of the mechanical deformation of the sample, indicating the component σ_{xx} of the stress tensor. The racetrack is patterned near the surface of the sample.*

In our work, we performed a time resolved electro-optic measurement of strained Si resonators to distinguish between the Pockels effect and the plasma carrier dispersion effect, since they have two different characteristic timescales. The first responds almost instantaneously to an applied electric field, while the second has a slower response, of the order of few nanoseconds. If the modulation period is decreased below this value, free carriers do not follow anymore the voltage variations, and, as a consequence, it is possible to isolate χ^2 effects. The high frequency meas-

urements are performed on racetrack resonators in the Add-Drop configuration, which are shown in fig. 21(a). The sample is strained by applying a mechanical deformation using a special sample holder. The resonator is excited by a continuous wave Infra-Red laser. The transmitted signal is recorded by a fast photodiode, of 40 GHz of bandwidth. A sinusoidal voltage is applied to the electrodes, because of the electro-optic modulation, the resonance wavelength follows the oscillations of the electric field, thus modulating the transmitted optical signal, at the same frequency of the applied voltage. The amplitude of this oscillation, which is proportional to the χ^2_{zzz} component, is recorded as the modulation frequency is increased from 50 MHz to 5 GHz. From this, the χ^2_{zzz} component is computed, which is shown in fig. 22. It is found that the value of the χ^2 monotonically decreases with frequency, from a value of $\sim 270\ pmV^{-1}$ at low frequency, to a value of $(8 \pm 3)\ pmV^{-1}$ at 5 GHz, which corresponds to the noise level of the apparatus. The cut-off frequency is $\nu_c = (0.50 \pm 0.01)\ GHz$, corresponding to a characteristic time of $\tau_c = (0.55 \pm 0.01)\ ns$. Surprisingly, the behavior of the χ^2 with frequency does not appreciably depend on the applied stress.

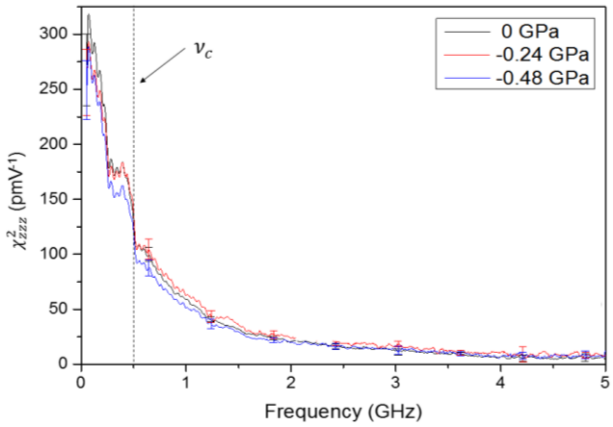

Figure 22. *Value of the χ^2_{zzz} component as a function of the voltage modulation frequency.*

From these considerations, it can be concluded that, in the low frequency region, the electro-optic modulation is caused by a dispersion mechanism having a timescale of the order of the nanosecond. This excludes the Pockels effect as the origin of the modulation, indicating that plasma carrier dispersion could be the dominating mechanism. We extract an upper limit of $(8 \pm 3)\ pmV^{-1}$ for the strain-induced χ^2in Si waveguides, which corresponds to our minimum detectable signal. This value is more than one order of magnitude lower than the one reported in the low-frequency regime in the literature [1,2,3].

References

1. R.S. Jacobsen, K.N. Andersen, P.I. Borel, J.Fage-Pedersen, L. H. Frandsen, O. Hansen, M. Kristensen, A.V. Lavrinenko, G. Moulin, H. Ou, C. Peucheret, B. Zsigri, and A. Bjarklev, Nature, 441, 199-202, (2006).
2. B. Chmielak, C.Matheisen, C. Ripperda, J. Bolten, T. Wahlbrink, M. Waldow, and Heinrich Kurz, Opt. Express, 21, 25324-25332, (2013).
3. P. Damas, X. Le Roux, D. Le Bourdais, E. Cassan, D. Marris-Morini, N. Izard, T. Maroutian, P. Lecoeur, and L. Vivien, Opt. Express, 22, 22095-22100, (2014).
4. S. Azadeh, F. Merget, M.P. Nezhad, and J.Witzens, Opt. Lett., 40, 1877-1880, (2015).

12. Four wave mixing in Si nanocrystal waveguides (Santanu Manna, Fernando Ramiro Manzano)

Non-linear silicon photonics is a rapidly emerging field drawing significant attention due to the possibility of all optical signal processing employing the existing mature planar Si technology. Owing to the significant optical non-linearities, Si nanocrystals (NCs) can be chosen as active material in non-linear photonic devices. A large third order non-linearity is possible for Si NCs because of both quantum confinement and dielectric mismatch phenomena. In parallel, the nonlinear losses due to the two-photon absorption (TPA) and excited carrier absorption (ECA) are often considered to be limiting factors. Here, we investigate degenerate four wave mixing (DFWM) in a Si NC stripe waveguide at 1550 nm, which will help in the assessment of Si NC nonlinearities.

Fabricated waveguides are based on a Si rich silica layer, deposited on a thermal oxide of 3 µm, which is annealed to form Si NCs. Finite element simulations (based on the COMSOL suite) were employed to obtain the modal behaviour of the waveguide. Inset of fig. 23(a) shows the modal profile for the fundamental TE mode. This gives a good confinement factor Γ of 0.86 but the effective area to be 1.01 µm^2, which is larger than reported Si waveguide. This waveguide exhibits a region of anomalous dispersion at 1550 nm. It results from a fine adjustment of the waveguide dimension and due to the presence of air as an upper cladding. The group index profile and the dispersion profile are shown in the fig. 23(b). It is noteworthy that Si NCs could act as scattering centers for light propagation in a waveguide, resulting in increased propagation losses. In our case, the propagation losses measured at 1550 nm are 3.0±0.2 dB/cm.

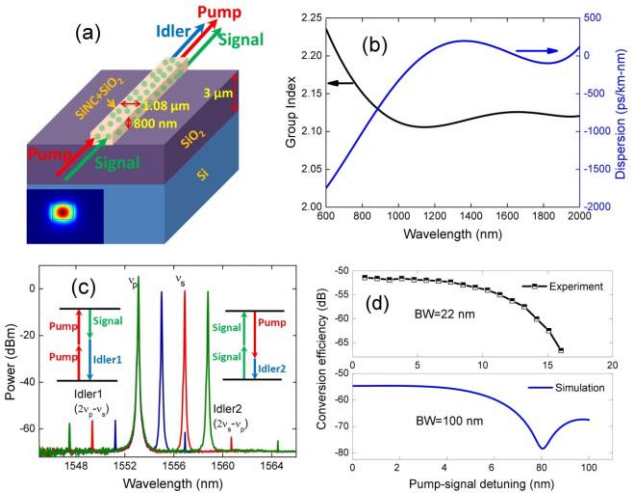

Figure 23. *(a) Schematic diagram of a Si NC stripe waveguide with dimension 800 nm×1080 nm on 3 µm thick silica; inset shows the TE fundamental mode profile. DFWM takes place in*

this waveguide while excited by a pump and a signal wavelength. (b) Calculated group index and group velocity dispersion D of the TE mode for the waveguide in (a). (c) Typical DFWM spectra for this waveguide with P_{pump} =31.8 mW and P_{signal} =5.9 mW. (d) Experimental as well as simulated signal to idler conversion efficiency as a function of the pump-signal detuning for this waveguide.

By studying the stimulated DFWM we make estimation of different nonlinear parameters: the nonlinear refractive index (n_2), the TPA coefficient (β_{TPA}), the excited carrier lifetime (τ), and the excited carrier cross section (σ_{ECA}). To extract these parameters, we model the DFWM process in a Si NC composite waveguide by nonlinear propagation equations. It is worth to mention that if β_{TPA}, n_2, and σ_{ECA} are for a single NC, $\xi\beta_{TPA}$, ξn_2 and $\zeta\sigma_{ECA}$ are the effective value for the Si NC/SiO_2 waveguide as a whole. The attenuation factors ξ, ζ attenuate the nonlinear parameters of the whole composite compared to those of the individual NC. In fact, these attenuation factors are dependent on the volume fraction (f) of Si in the matrix. For the present waveguide, values of f, ξ and ζ are calculated to be 28.4%, 0.041 and 0.196, respectively. Due to the important role of excited carriers, we performed a detailed measurement of the excited carrier losses. Using Γ =0.86 at 1550 nm for the TE polarized fundamental mode, effective carrier absorption cross section $\zeta\sigma_{ECA}$ was found to be 2.5±1.0 $\times 10^{-20}$ cm^2 when the density of NCs is 3.5×10^{18} cm^{-3}. The carrier lifetime extracted from experiment is 3±1 µs.

Stimulated DFWM measurements have been performed on 5 mm long waveguides by fixing the pump wavelength at 1550 nm and by varying the signal wavelength in a range from 1550 to 1575 nm. In the parametric DFWM process, the energy conservation is strictly maintained. Thus, the frequency of the idler is determined by the frequency difference between pump and signal frequencies $\nu_{idler} = 2\nu_p - \nu_s$, (ν_p, ν_s and ν_{idler} being the frequency of the pump, signal, and idler). If the signal is strong another idler may appear at a frequency $\nu_{idler2} = 2\nu_s - \nu_p$. Typical FWM spectra are shown in the fig. 23(c). By fitting the parameters to the experimental data (signal to idler conversion ratio), we have extracted a value of ξn_2 =3.8±0.7×10^{-18} m^2/W, $\xi\beta_{TPA}$ =3±1×10^{-10} m/W, $\zeta\sigma_{ECA}$ =3.5±1×10^{-20} cm^2 and τ =4±3 µs. Fitted $\xi\beta_{TPA}$ as well as $\zeta\sigma_{ECA}$ values agree well with the experimentally measured values. The above nonlinear absorption processes could limit the nonlinear conversion processes. This can be quantified by the characteristic figure of merit FOM= $n_2 / \lambda\beta_{TPA}$ which is calculated to be 0.007±0.003 for the present waveguide. This value is ~50 times lower than the one for Si waveguides. Figure 19(d) presents the measured conversion bandwidth of the Si NC waveguide. The highest conversion efficiency is -51.4 dB, and -3 dB bandwidth is 22 nm. We found theoretically that the larger is the carrier lifetime, the lower is the signal to idler conversion efficiency. The bandwidth is mostly unaffected by the carrier lifetime since it depends on the dispersion and length of the waveguide. Surprisingly, the measured conversion bandwidth are narrower than the simulated value (100 nm), but more than the reported conversion bandwidth of 10 nm in a horizontal slot Si NC waveguide.

For more info

Nanoscience Laboratory
Department of Physics
University of Trento
via Sommarive 14
38123 Povo- Trento (Italy)
http://nanolab.physics.unitn.it/

secretary dr. Tanya Yaksevich
email tatsiana.yatckevich@unitn.it
phone +390 461 283172